JOURNAL OF SOLID STATE CHEMISTRY **136,** 167–174 (1998)
ARTICLE NO. SC977670

# Comparison of the Properties of Bismuth Sulfide Thin Films Prepared by Thermal Evaporation and Chemical Bath Deposition

M. E. Rincón,[1] M. Sánchez, P. J. George, A. Sánchez, and P. K. Nair

*Centro de Investigación en Energia, Universidad Nacional Autónoma de México, 62580 Temixco, Morelos, Mexico*

Received July 17, 1996; in revised form October 16, 1997; accepted October 23, 1997

**Highly oriented polycrystalline $Bi_2S_3$ thin films with crystallinities superior to those obtained in chemically deposited $Bi_2S_3$ thin films were prepared by direct evaporation of bismuth sulfide precipitate. The XRD patterns of these films show preferential growth of bismuth and bismuthinite planes, and this growth could be correlated to substrate temperature and substrate type. For films deposited on glass substrates at room temperature, the XRD pattern shows an incipient growth of $Bi_2S_3$ (bismuthinite) along the [020], [220], and [021] directions. At these angles, Bi planes also diffract and might be the major component of this alloy. XRD spectra of films deposited on bare glass in the substrate temperature range 150–300°C show that the film growth evolves from an oriented to a more random pattern. At a substrate temperature of 250°C, the crystallization of bismuth and bismuthinite is accelerated on glass substrates with a Cr coating and inhibited on glass substrates with a $SnO_2$ coating. The reflectance spectra of the films deposited at 250°C on uncoated and $SnO_2$-coated glass substrates show that the crystallinity is dominated by $Bi_2S_3$, whereas in films deposited on a Cr grid Bi is a strong component. The optoelectronic properties of the deposited films indicate very conductive layered structures with $E_g$ values in the range 1.2–1.6 eV. Compared with the above, chemically deposited thin films were less crystalline and more stoichiometric, with a lower conductivity and higher optical band gap (1.5–2.0 eV). The possible application of these films in heterojunction and photoelectrochemical devices is suggested.** 

## 1. INTRODUCTION

Bismuth sulfide thin films have been obtained by a variety of techniques (1–9) due to their importance as a semiconductor material for application in optoelectronic, thermoelectric, and photoelectrochemical devices. The optical band gap ($E_g$) of $Bi_2S_3$ reported by different authors is in the range of 1.2–1.84 eV, but the variation in the values does not seem to be correlated to the amorphous or polycrystalline nature of the deposited film. In our laboratory, specularly reflective bismuth sulfide thin films have been obtained by chemical bath deposition (10–13) and, more recently, by low-temperature–low-vacuum vapor phase deposition (14). We have reported that chemical bath deposition renders bismuth sulfide films that are amorphous in the as-deposited form and that these films undergo an irreversible amorphous to crystalline transformation during postdeposition thermal treatments at or above 200°C (11). On the other hand, the films obtained by the low-temperature–low-vacuum vapor phase deposition from bismuth sulfide precipitate are highly polycrystalline (14). Such films show a trend of decreasing $E_g$ with increasing substrate temperature ($T_{sub}$). Furthermore, in this vapor phase deposition technique substrate temperatures were found to govern the stoichiometry of the deposited films more strongly than the source composition.

To investigate the effect of source temperature and pressure on the properties of bismuth sulfide films deposited by thermal evaporation, in this article we report the results of direct evaporation of the nearly stoichiometric bismuth sulfide precipitate as used in the low-temperature studies (14). In the present case evaporation takes place in a vacuum chamber under substantially higher temperature (900 vs 500°C) and higher vacuum ($10^{-6}$ vs 30 mbar) than in previous studies (14). The source temperature is important in determining the $E_g$ values of metal chalcogenides deposited by direct evaporation (15). The $E_g$ of $Sb_2Se_3$, for example, was reported to decrease monotonically with increasing source temperature. The reason given was that below the melting point of $Sb_2Se_3$, the Se/Sb ratio is higher than stoichiometric, and the $E_g$ of the alloy is in between the $E_g$ of Se and $Sb_2Se_3$. Similarly, above the melting point, the Se/Sb ratio is lower than stoichiometric; thus the deposited films have band gaps lower than that of stoichiometric $Sb_2Se_3$.

For the films deposited by the method described here, high-temperature–high-vacuum deposition, the correlation of the optical band gap, stoichiometry, and orientation of the films with substrate temperature and substrate type was examined. As in the case of the low-temperature–low-vacuum vapor phase deposition (14), the substrate temperature

[1] Author to whom correspondence should be addressed.



0022-4596/98 $25.00

was found to be an important control parameter to ensure proper composition of bismuth sulfide films. The structure and composition of the films obtained by thermal evaporation (both high temperature–high vacuum, and low temperature–low vacuum) were compared to those obtained by chemical deposition. The role of varying amorphicity and stoichiometry in determining the properties of the films is also discussed, along with potential applications of the developed material.

## 2. EXPERIMENTAL

### *Chemically Deposited Precipitate and Films*

The source utilized in thermal evaporation was a bismuth sulfide precipitate obtained as a byproduct in chemical bath deposition of thin films. Details of the preparation of the chemical bath are given elsewhere (10). The deposition bath had a basic pH and contained 0.05 M $Bi^{3+}$, 0.6 M triethanolamine, and 0.04 M thioacetamide as the source of $S^{2-}$. After 24 h at 25°C, the precipitate was filtered and dried at room temperature, while the deposited films ($\sim 0.2$ μm) were rinsed and subjected to thermal treatments in inert environments. About 100 mg of the chemically precipitated powder was transferred into a closed tungsten crucible attached to copper feedthroughs inside a commercial thermal evaporator. A vacuum of $2 \times 10^{-6}$ mbar was established before the source temperature was raised to 800–900°C. Three kinds of glass substrates were investigated: microscope glass, commercially coated $SnO_2$ glass, and glass/Cr grids. They were placed 12 cm above the source and were kept at a prefixed temperature during the 4–8-min evaporation time.

### *Film Characterization*

The X-ray diffraction (XRD) patterns of the films were recorded using a Siemens D 5000 system with Cu$K\alpha$ radiation. Coplanar silver print electrodes with a square geometry (5 mm long at 5-mm separation) were applied on the film surface to measure the photocurrent response. Measurements were made at a bias of 10 V with a computerized system (16) and with a halogen–tungsten lamp that provided illumination intensities of 200 W/m$^2$ over the plane of the sample. The optical transmittance and near-normal specular reflectance spectra were recorded on a Shimadzu UV 3101 near-infrared UV–vis spectrophotometer for film-side and substrate-side incidence.

The thicknesses of the chemically deposited and evaporated thin films were determined using an Alpha Step 100 unit.

## 3. RESULTS AND DISCUSSION

### *Structural Characterization of Evaporated Films*

The conditions of deposition and the thicknesses of the deposited films are given in Table 1. In cold substrates the thickness of the deposited film is $\sim 0.07$ μm and goes through a maximum as the substrate temperature increases. The maximum thickness obtained was 0.12 μm at 200°C. The structural features of films deposited at various substrate temperatures by thermal evaporation are shown in Fig. 1. The peaks observed in all patterns can be matched with diffractions due to Bi (JCPDS 5-0519) and $Bi_2S_3$ (JCPDS 17-0320). In the XRD pattern of the film deposited at 25°C, the relative intensities of the peaks are weak. For substrate temperatures of 200°C and above, XRD peaks corresponding to several planes of $Bi_2S_3$ appear while the peak of the combined diffraction of Bi and $Bi_2S_3$ at $2\theta \sim 27°$ decreases. At $T_{sub} = 300$°C, the presence of Bi in the film is indicated by the XRD peak due to the (104) planes of bismuth. The contribution of Bi to the XRD peaks common to Bi and $Bi_2S_3$ seems to decrease. At high substrate temperatures the reaction of bismuth and sulfur to produce $Bi_2S_3$ seems to be fast enough to promote growth in several directions and the XRD pattern of $Bi_2S_3$ is well resolved at all angles, resembling the pattern of the powder. The thickness reduction of the films deposited at 300°C can account for the lower intensity of the XRD pattern.

Figure 1 indicates that some Bi planes determine the preferential growth of the $Bi_2S_3$ crystallites, since the XRD peaks due to the (220) and (021) planes of $Bi_2S_3$ have unusually high intensities compared to the diffraction pattern of the powder. The preferential growth of the $Bi_2S_3$ crystallites has also been observed in films prepared by other gas-phase deposition techniques in XRD peaks located at $2\theta < 25°$. Films obtained by reactive evaporation (9) and films grown from a sulfur-rich vapor phase (14) have XRD patterns in which the strongest bismuthinite diffractions correspond to the (130) and (310) planes. Other important diffracting planes were the (020) (14) and (220) (9), all located at $2\theta < 25°$. This could be indicative of the lack of long-range order in the films.

**TABLE 1**
**Deposition Conditions and Thickness of Bismuth Sulfide Thin Films Obtained by Thermal Evaporation of a Bismuth Sulfide Precipitate[a]**

| Substrate | $T_{sub}$ (°C) | $t_{dep}$ (min) | Thickness (Å) ± 200 | Deposition rate (Å/min) |
|---|---|---|---|---|
| Glass | 25 | 4 | 700 | 175 ± 50 |
| Glass | 150 | 4 | 900 | 225 ± 10 |
| Glass | 200 | 4 | 1200 | 300 ± 10 |
| Glass | 250 | 4 | 900 | 225 ± 10 |
| Glass | 300 | 4 | 600 | 150 ± 10 |
| Glass | 250 | 8 | 1128 | 141 ± 20 |
| Glass/$SnO_2$ | 250 | 8 | 1128 | 141 ± 20 |
| Glass/Cr | 250 | 8 | 1128 | 141 ± 20 |
| *Glass* | *25* | *1320* | *2000* | *1.5 ± 0.2* |

[a]Data for the films obtained by chemical bath deposition are given in italics for comparison.

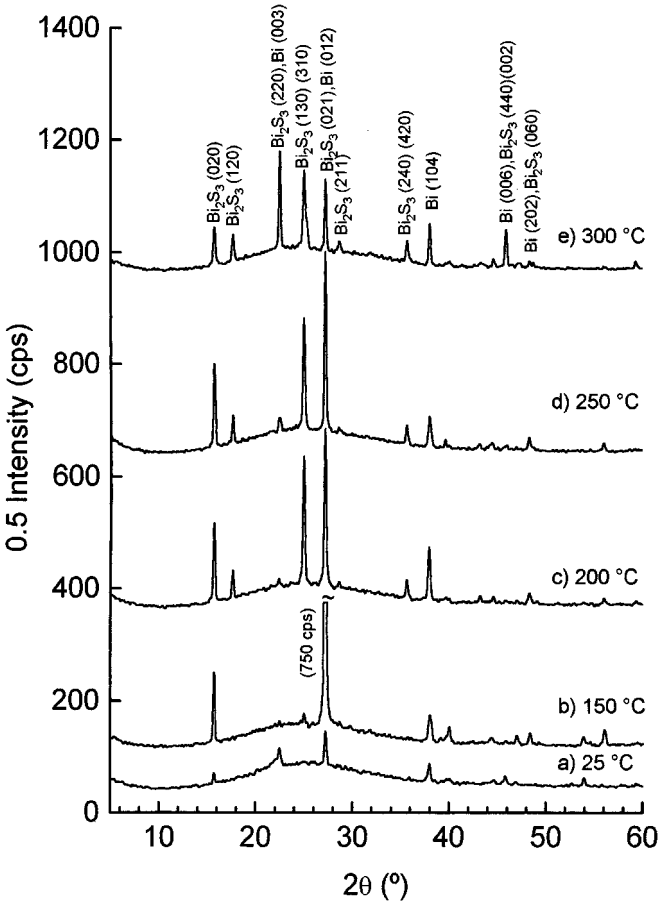


**FIG. 1.** Cu$K\alpha$ XRD patterns of films deposited on glass substrates by thermal evaporation of a chemically deposited bismuth sulfide precipitate. Substrate temperatures ($T_{sub}$): (a) 25, (b) 150, (c) 200, (d) 250, and (e) 300°C. Duration of deposition: 4 min.

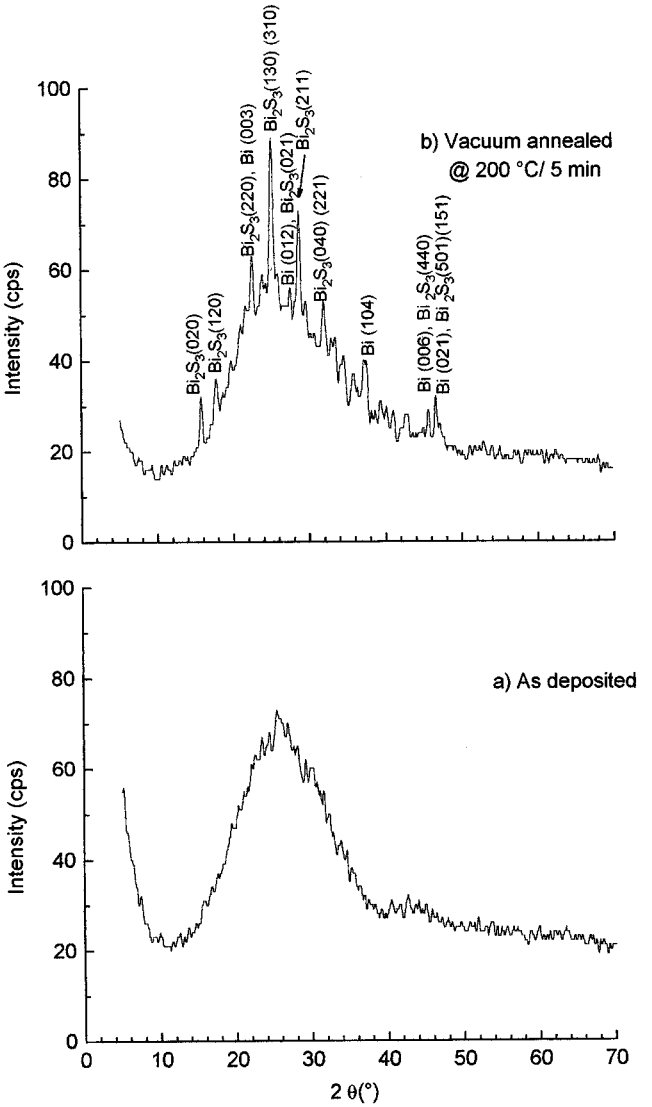


**FIG. 2.** Cu$K\alpha$ XRD patterns of films deposited on glass substrates from a chemical bath: (a) as-deposited film; (b) vacuum-annealed film at 200°C in an Ar atmosphere for 5 min.

Comparison of the patterns shown in Fig. 1 indicates that, regardless of the high source temperature, sulfur and bismuth atoms or molecules are effectively quenched on the cold substrate. The chemical reaction giving bismuthinite (17) is very inefficient below 150°C. Sulfur remains as a component in a low-order bismuth sulfide in the amorphous phase. The presence of a maximum in film thickness vs $T_{sub}$ (Table 1) can be explained in terms of the competition between the rate of sulfur evaporation and the rate of chemical reaction.

*Structural Characterization of Chemically Deposited Films*

The XRD patterns of as-deposited and vacuum-annealed films obtained from a chemical bath (24-h deposition at 25°C) are shown in Fig. 2. Figure 2a indicates the amorphous nature of the 0.2-μm-thick chemically deposited films. They become crystalline after annealing at around 200°C in several environments (Ar, $H_2$, $O_2$, air, vacuum, and atmospheric pressure) (12, 13). The pattern shown in Fig. 2b is representative of the crystallinity induced by postdeposition thermal treatments around 200°C. The thickness of the annealed films is ~0.13 μm. According to this figure, the preferential orientation of $Bi_2S_3$ planes is minimal. The XRD pattern of the film resembles the standard powder XRD pattern (JCPDS 17-0320) remarkably well.

Comparison of Figs. 1c ($T_{sub}$ = 200°C) and 2b ($T_{annealing}$ = 200°C) indicates that, regardless of the thickness of the evaporated films, the films obtained by thermal evaporation are more crystalline and more highly oriented than the chemically deposited films. Comparison of Figs. 1a ($T_{sub}$ = 25°C) and 2a (chemically deposited film without thermal treatment) is difficult because of the lack of evidence

for any structure in the chemically deposited film. From past work (11–13) we know that chemically deposited films are highly stoichiometric (as-deposited), whereas XRD spectra of films deposited at 25°C by thermal evaporation (Fig. 1a) indicate a nonstoichiometric crystalline alloy, rich in bismuth. Similar conclusions regarding intensity, stoichiometry, and orientation hold when the evaporated films are compared with chemically deposited films obtained at pH ~ 1–3. It was observed that the as-deposited crystallinity of the films obtained from the chemical bath depends strongly on the pH of the solution (4–5, 7–8, and 11). Amorphous material (films and precipitate) is obtained with basic baths and polycrystalline material with acidic baths. As in the case of the films obtained from basic solutions and subjected to argon annealing (Fig. 2b), the XRD patterns of the as-deposited polycrystalline material obtained in acidic formulations have low intensity and sufficiently strong (130), (310), and (211) bismuthinite planes to keep a close resemblance to the XRD pattern of the powder. Therefore, when compared with chemically deposited films, the evaporated films are more crystalline but nonstoichiometric and highly oriented.

*Electrical Characterization: The Role of Stoichiometry and Amorphicity*

The photocurrent response of the films deposited by thermal evaporation at various substrate temperatures is given in Fig. 3 along with those of as-deposited and vacuum-annealed films obtained from a chemical bath. High conductivity and zero photoresponse are observed in the films obtained by thermal evaporation at $T_{sub}$ below 250°C. Lower conductivity and some photosensitivity are observed in films deposited at 250 and 300°C. The photocurrent response of the films obtained from the chemical bath (after postdeposition thermal treatments at 200°C) given in Fig. 3 can be compared with the one obtained by thermal evaporation at $T_{sub} = 300$°C. The high conductivity of these films, along with the XRD patterns (Figs. 1 and 2), indicates the strong role of the bismuth component, either as a second

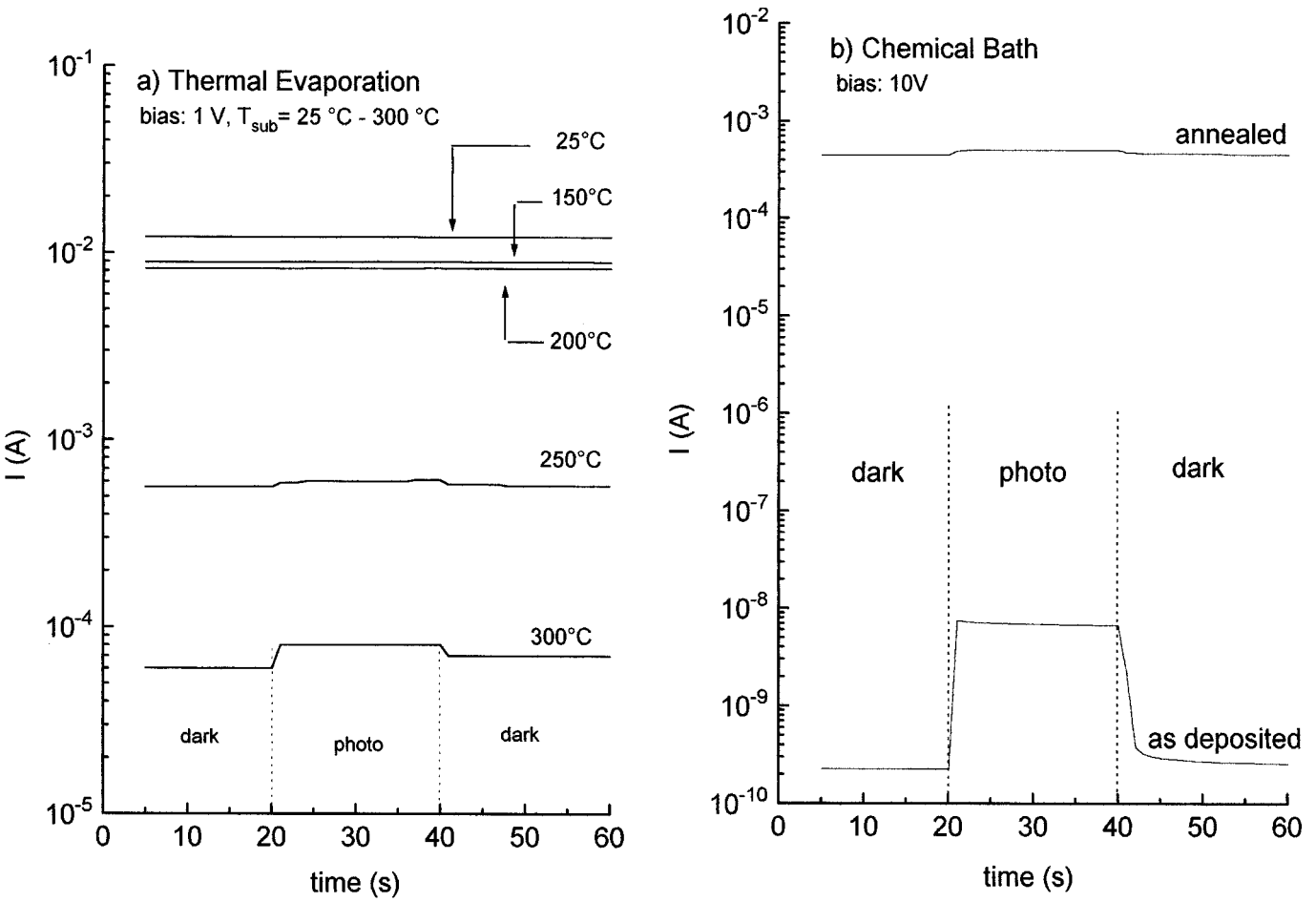


**FIG. 3.** Photocurrent response of films obtained by (a) thermal evaporation for 4 min at various substrate temperatures and (b) chemical bath deposition with and without argon annealing ($10^{-2}$ torr) at 200°C for 5 min.

crystalline phase or as a strong dopant/modifier in the crystalline/amorphous $Bi_2S_3$ phase.

*Stoichiometry.* For the films obtained by thermal evaporation and deposited on substrates at temperatures below 200°C, it is reasonable to assume that an important contribution to the diffraction observed at $2\theta \sim 28^\circ$ comes from the (012) plane of Bi. As the deposition temperature increases, the $Bi/Bi_2S_3$ ratio decreases, causing the dark conductivity to decrease and the $I_{ph}/I_d$ ratio (photocurrent vs dark current) to increase.

On the other hand, the presence of bismuth is indicated by minor peaks in the XRD spectrum of chemically deposited films after thermal treatments in inert environments [bismuth planes (012), (104), and (006) in Fig. 2b]. Even though some of the bismuth and bismuthinite planes overlap, the intensities of the combined diffractions are low. Among the Bi planes that do not overlap is the (104) plane. This diffraction at $2\theta \sim 38^\circ$ suggests that the $Bi/Bi_2S_3$ ratio is comparable in the argon-annealed chemically deposited film and the evaporated film deposited at 300°C. In other words, the S/Bi ratio goes up in Figs. 3a and 3b from top to bottom.

With the exception of the as-deposited and highly stoichiometric amorphous film obtained from the chemical bath at basic pH, the conductivities of the argon-annealed and evaporated films are high, in the $1–100\,\Omega^{-1}\,cm^{-1}$ range. Additionally, the as-deposited stoichiometric polycrystalline material obtained from acidic baths have conductivities on the order of $10^{-5}\,\Omega^{-1}\,cm^{-1}$ (8). This indicates that charge transport is dramatically affected by the nonstoichiometry of the films. We have reported before (12) that even very low concentrations of bismuth can trigger high conductivity in a two-phase system through percolation mechanisms.

*Amorphicity.* The degree of crystallinity varies between deposition at 25°C and thermal treatments (or deposition) at higher temperatures (Fig. 1a vs 1b–e, Fig. 2a vs 2b). It also varies between chemically deposited films and evaporated films (Fig. 1b vs 2b–e). It is well known that the compositional or positional disorder increases from elemental to compound to alloy materials. Extensive work on amorphous material indicates that, although the optical properties are determined by the normal structural bonding (NSB), the electrical properties are controlled by the deviant electronic configurations (DECs) (19). These DECs are very different in crystalline semiconductors and amorphous solids. As a consequence, the presence of Bi can trigger extrinsic conduction either as a segregated phase (percolation), as a dopant in crystalline $Bi_2S_3$ (*n*-type conductivity), or as a modifier in amorphous $Bi_2S_3$ (*n*-type conductivity by overcoordination, charge compensation, etc.) (19).

The transition from amorphous to crystalline form enhances the long-range order dramatically and usually results in a large increase in dark conductivity. The effects of the transition, or the transition itself, can be overtaken by the presence of modifiers. Consequently, the nonstoichiometric condition of the bismuth sulfide films seems to be far more important in determining the electrical properties than their amorphous or crystalline states. This would explain the large resistivity reported for stoichiometric amorphous and polycrystalline films (8–10).

### *Optical Characterization*

The films obtained by thermal evaporation at different substrate temperatures appear significantly different when observed from the substrate side (ss) or film side (fs). At $T_{sub} = 25°C$, the films appear dark from the ss but possess a metallic luster from the fs. In the case of $T_{sub} = 300°C$, the appearance is reversed. In chemically deposited film, the appearance is nearly identical for ss and fs incidence. Figure 4 shows the near-normal specular reflectance spectra of the films. The optical interference peaks are notable in the case of ss incidence in the evaporated films. The difference in the reflectance spectra in the two modes of incidence suggests that there exists compositional changes in the film during deposition. This arises due to nonstoichiometric dissociation (bismuth enrichment of the source) and/or variable sticking coefficients for the incoming ions depending on the composition of the film surface just formed.

As discussed in the previous section, the degree of amorphicity is not expected to have a strong role in determining an overall displacement or large magnitude change in the curves of optical constants vs photon energy (19, 20). The NSB, determined by the atom itself and its coordination to its nearest neighbors, controls the optical behavior. Since the local order, the bond lengths, and the bond angles are not expected to be very different in the amorphous and crystalline compounds (they mainly differ at long range), both states are expected to have similar optical behavior (19). In contradiction with this, some authors have shown that the dielectric constant can change strongly from one phase to the other in some spectral regions (20). Furthermore, due to the capability of the majority of atoms to incorporate as multivalent states, alloys can cause important changes in the coordination to nearest neighbors, creating a whole new set of NSB and DECs.

In our work we found that some features observed in Fig. 4 can be explained in terms of amorphous or crystalline forms, but others in terms of compositional changes. At low photon energies (below $E_g$), we expect that the index of refraction of bismuth will determine the reflectivity of the film. At the low-energy end, the high fs reflectivity of the evaporated samples deposited at the lowest temperatures (Fig. 4a) can be explained in terms of higher Bi content (inefficient chemical reaction below 200°C). On the other hand, the difference in fs reflectance between the evaporated

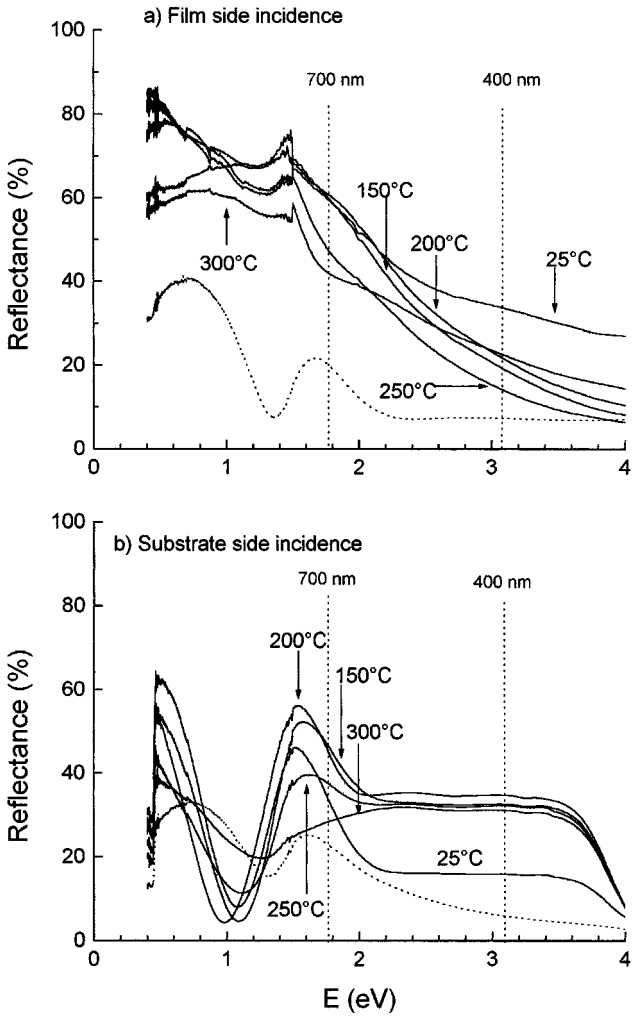


**FIG. 4.** Reflectance spectra of films deposited at various substrate temperatures (25–300°C) by thermal evaporation for 4 min recorded for (a) film-side (fs) light incidence and (b) substrate-side (ss) light incidence. Dotted lines refer to the reflectance spectra of films deposited from a chemical bath for 22 hr at 25°C.

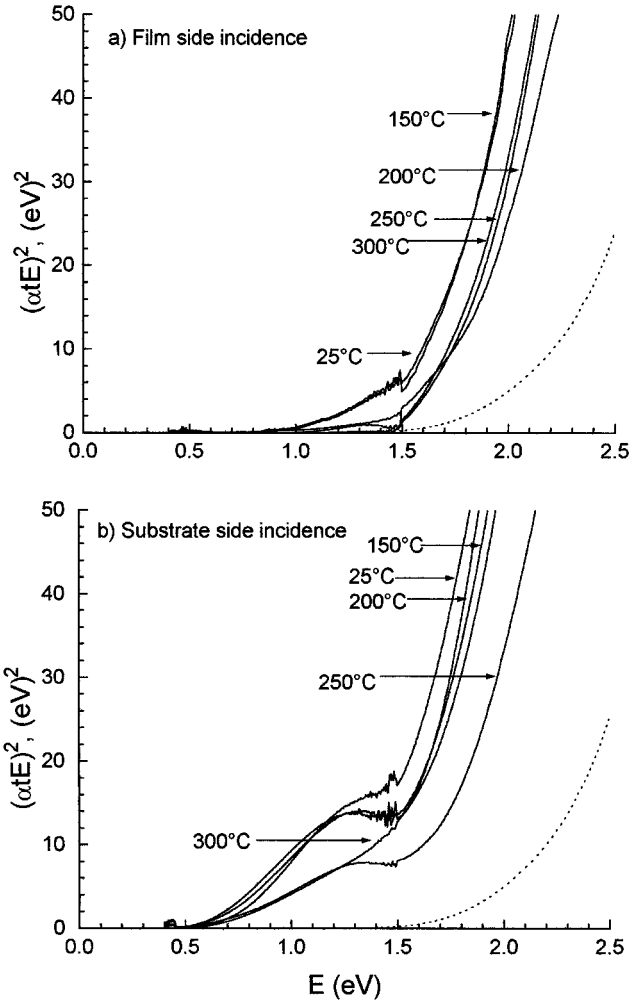


**FIG. 5.** Plots of $(\alpha tE)^2$ vs photon energy $E$ of the films in Fig. 4. The band gap for direct transitions is the intercept obtained by extrapolation of the linear portion of the curve to the energy axis.

sample deposited at 300°C (Fig. 4a) and the as-deposited amorphous film (dotted line in Fig. 4a) is more likely to be due to the differences in crystallinity and thickness since both samples are close to the stoichiometric S/Bi ratio.

The band gaps of the films were determined from the equation describing optical absorption of direct transitions in crystalline materials. Figure 5 shows a plot of $(\alpha tE)^2$ vs $E$, where $\alpha$ is the absorption coefficient, $t$ the thickness of the absorbing layer, and $E$ the photon energy. The product $\alpha t$ was obtained from transmittance spectra after correcting for front-surface reflection (21). It is clear from this figure that the chemically deposited films (amorphous material) are the most transparent ($E_g$ (band gap) $> 2$ eV) whereas the films deposited at the lowest temperatures are the most opaque ($E_g = 1$ and 1.4 eV) with a pattern showing strong absorbency at low energies (metallic behavior). The curves of the films deposited at 200°C or above give $E_g$ values of 1.5 eV.

Since the equation described is not appropriate for amorphous films, we also plotted $(\alpha tE)^n$ vs $E$ with $n = 1, \frac{1}{2}$, and $\frac{1}{3}$ (22) for the chemically deposited films. The linearity of the curves obtained was very poor for $n = \frac{1}{2}$ and $\frac{1}{3}$ and gave values of $E_g$ below 1 eV. The plot of $(\alpha tE)$ vs $E$ gave two linear regions with intercepts at 1.4 and 1.8 eV. The superior linearity of the curves obtained when using the equation for crystalline material ($n = 2$) strongly suggests that the size of the crystallites in the chemically deposited films is too small to be resolved in XRD and that the shift to higher optical band gap values (from 1.5 to 2 eV) might be due to quantization effects, that is, the common blue shift observed in nanoparticles (23).

In summary, the optical band gaps ($E_g \sim 1.5$–$1.6$ eV) and absorption coefficients ($\alpha \sim 10^5\ cm^{-1}$) of the films obtained on substrates above 200°C by evaporation of bismuth sulfide precipitate at 900°C compare well with the ones obtained by evaporation of the same precipitate at 500°C and deposited in substrates held at 290–345°C ($E_g \sim 1.2$–$1.4$ eV; $\alpha \sim 10^5\ cm^{-1}$) (14). In both cases the crystallinity of the films was good, but the stoichiometry is superior in the low-temperature deposition method. The expected effect of lower $E_g$ due to higher source temperature was observed in the films deposited with substrate temperatures below 200°C and gives rise to two linear regions in the $(\alpha h\nu)^2$ vs $h\nu$ curve, where the $x$ intercept gives $E_g$ values of 1 and 1.4 eV. Comparison of both deposition techniques at the same substrate temperature suggests higher $E_g$ for the high-temperature–high-vacuum method (contrary to what was expected).

### *Substrate Effects*

To observe the effect of different substrates on the sticking coefficient of S/Bi, the deposition was made on uncoated glass substrates and on conductive $SnO_2$-coated glass and Cr-coated glass substrates. The source temperature was 800–900°C, the same as before (Table 1 and Fig. 1), but instead of a closed tungsten crucible, we used open graphite crucibles and longer evaporation times (8 vs 4 min).

With 8 min of deposition time at a substrate temperature of 250°C, the thickness of the films deposited on the three different substrates was about 0.1 μm. However, regardless of the nearly identical thickness, the XRD patterns of the films deposited on different substrates are very different. Figure 6 shows the XRD patterns after elimination of the background. As seen in Figs. 1 and 2, the background accounts for $<50$ cps and is mainly due to the glass substrate in the case of these films. Figure 6 indicates that if the deposition takes place on glass substrates coated with Cr, the crystallization of Bi is accelerated and the crystallites are highly oriented along the $c$ axis (strong peaks at $2\theta = 22.5°$ and 46°, the (003) and (006) planes of Bi). If the glass substrate is coated with $SnO_2$, the XRD pattern of the deposited films shows that the bismuth and bismuthinite peaks are smaller than the ones obtained from films deposited on uncoated glass substrates and on substrates coated with Cr. This indicates that either the crystallization of Bi or the reaction between Bi and S is inhibited on an $SnO_2$ substrate. One reason for the preferred growth on the Cr substrate might be the likely presence of $Cr_2O_3$ in the coated glass (a common problem in chromium coating at low pressure). The crystalline structures of $Cr_2O_3$ (hex-R, *R*3*c* (No. 167)), Bi (hex-R, *R*3*m* (No. 166)), and S (hex-R, *R*3 (No. 148)) are very similar, and the chromium oxide could be a better nucleation site for the initiation of the deposition than $SnO_2$ (tetra, *P*4/*mmm* (No. 136)). The mismatch in lattice structure between the elements and $Bi_2S_3$ (orthorhombic, *Pbnm* (No. 62)) could be one reason for the strong orientation of $Bi_2S_3$ planes observed in the XRD patterns of films obtained at 250°C. As in the case of Fig. 6a, the more prominent diffractions in Figs. 6b and 6c correspond to combined diffractions of Bi and $Bi_2S_3$.

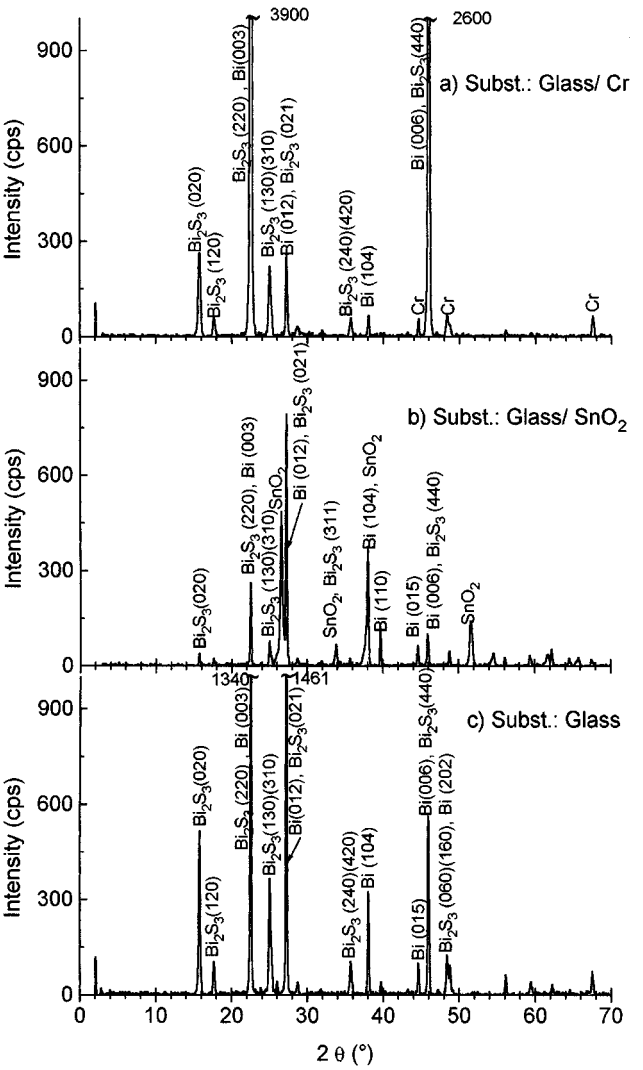


**FIG. 6.** Cu$K\alpha$ XRD patterns of films deposited by thermal evaporation of the bismuth sulfide precipitate on different substrates at 250°C for 8 min: (a) glass with Cr coating; (b) glass with $SnO_2$ coating; (c) uncoated glass.

### *Potential Applications of the Deposited Films*

Due to the high crystallinity and orientation of the films, we believe that the deposition parameters may be adjusted to have layered structures like Bi/*n*-$Bi_2S_3$ (bismuth rich)/*i*-$Bi_2S_3$ in a single evaporation. This might be accomplished by having a decreasing $T_{sub}$–time profile and by keeping the evaporation time short. The optimization of deposition

time, substrate material, and substrate temperature for the specific application of these films in heterojunctions and photoelectrochemical devices is currently under investigation. In photoelectrochemical cells, a layered structure like Bi/*n*-$Bi_2S_3$/*i*-$Bi_2S_3$ will enhance the *I–V* characteristics of the cell by increasing the photosensitivity and width of the absorbing layer (intrinsic material) and still provide enough band bending (difference between the Fermi level of the *n*-type material and the redox potential of the electrolyte) at the semiconductor–electrolyte interface. Similarly, we expect that the preferential growth of the different planes in bismuthinite may modify the chemical stability of the semiconductor in contact with the electrolyte.

## 4. CONCLUSION

In this paper we have illustrated that bismuth sulfide thin films of varying structure and composition can be prepared by thermal evaporation using bismuth sulfide powder (obtained from chemical precipitation) as the evaporation source. The material obtained at substrate temperatures below 200°C was a highly conductive Bi-rich Bi–$Bi_2S_3$ alloy with high reflectance below 1.4 eV and an optical band gap of 1–1.4 eV. At higher substrate temperatures (250–300°C), crystallization is enhanced and the formation of $Bi_2S_3$ promoted. The resulting films show lower dark conductivity (still above $1\ \Omega^{-1}\,cm^{-1}$), have lower reflectance, and produce XRD patterns with diffractions at all $Bi_2S_3$ planes. The patterns, however, show strong orientation effects and/or contribution of the (104), (012), and (003) planes of Bi. Films obtained above 200°C had optical band gaps of 1.5–1.6 eV and absorption coefficients on the order of $10^5\ cm^{-1}$. These values compare well with the 1.38 eV reported for films obtained by reactive evaporation (9). Due to nonstoichiometric dissociation of the precipitate, the S/Bi ratio in the source goes down with evaporation time, resulting in layers of varying composition in the deposited material. The changes can be compensated or enhanced by proper selection of evaporation time and substrate temperatures.

When compared with films obtained by chemical deposition (either argon-annealed when deposited from basic baths or as-prepared when deposited from acidic baths), chemically deposited films were less crystalline and more stoichiometric, with a lower conductivity and higher optical band gap (1.5–2.0 eV) (5, 7, 8).

The layered material obtained by evaporating $Bi_2S_3$ precipitate at 900°C and $10^{-6}$ mbar resembles the material obained by evaporating the same precipitate at 500°C and 30 mbar reported before (14). The expected effect of lower $E_g$ due to higher source temperature was observed at the lowest substrate temperatures (25–150°C) in our studies. Comparison of films obtained by both evaporation techniques (high and low source temperature) at the same substrate temperature did not show the mentioned effect. We are currently working at optimizing the composition of the layered structure in the developed material for use in photoelectrochemical cells.

## ACKNOWLEDGMENTS

The authors are grateful to L. Baños for the XRD analyses and DGAPA–UNAM (Mexico) for financial support.

## REFERENCES

1. B. Miller and A. Heller, *Nature* **262,** 680 (1976).
2. A. S. Baranski, W. R. Fawcett, and C. M. Gilbert, *J. Electrochem. Soc.* **130,** 2423 (1983).
3. R. N. Bhattacharya and P. Pramanik, *J. Electrochem. Soc.* **129,** 332 (1982).
4. S. Biswas, A. Mondal, D. Mukherjee, and P. Pramanik, *J. Electrochem. Soc.* **133,** 48 (1986).
5. C. D. Lokhande, V. S. Yermune, and S. H. Pawar, *Thin Film Prep.* **135,** 1852 (1988).
6. S. Misra and H. C. Padhi, *J. Appl. Phys.* **75,** 4576 (1994).
7. J. D. Desai and C. D. Lokhande, *Indian J. Pure Appl. Phys.* **31,** 152 (1993).
8. J. D. Desai and C. D. Lokhande, *Mater. Chem. Phys.* **41,** 98 (1995).
9. J. Lukose and B. Pradeep, *Solid State Commun.* **78,** 535 (1991).
10. M. T. S. Nair and P. K. Nair, *Semicond. Sci. Technol.* **5,** 1225 (1990).
11. P. K. Nair, J. Campos, A. Sánchez, L. Baños, and M. T. S. Nair, *Semicond. Sci. Technol.* **6,** 393 (1991).
12. M. E. Rincón and P. K. Nair, *J. Phys. Chem. Solids* **57,** 1937 (1996).
13. M. E. Rincón, R. Suárez, and P. K. Nair, *J. Phys. Chem. Solids* **57,** 1947 (1996).
14. M. E. Rincón and P. K. Nair, *Semicond. Sci. Technol.* **12,** 467 (1997).
15. A. Efstathion, D. M. Hoffman, and E. R. Levin, *in* "Extended Abstracts of the 13th AVS Symposium," p. 143. Herbick and Held Printing Co., Pittsburgh, PA, 1966.
16. P. K. Nair, J. Campos, and M. T. S. Nair, *Semicond. Sci. Technol.* **3,** 134 (1989).
17. A. Glatz and V. F. Meikleham, *J. Electrochem. Soc.* **110,** 1231 (1963).
18. J. C. Schottmiller, F. Ryan, and T. Taylor, *in* "Extended Abstracts of the 14th AVS Symposium," p. 29. Herbick and Held Printing Co., Pittsburgh, PA, 1967.
19. S. R. Ovshinsky and D. Adler, *Contemp. Phys.* **19,** 109 (1978).
20. J. Feinleib and S. R. Ovshinsky, *J. Non-Cryst. Solids* **4,** 564 (1970).
21. S. Perkowitz, "Optical Characterization of Semiconductors: Infrared, Raman and Photoluminescence Spectroscopy." Academic Press Inc., San Diego, CA, 1993.
22. J. Tauc, "Amorphous and Liquid Semiconductors." Plenum, New York, 1974.
23. A. Henglein, *Chem. Rev.* **89,** 1861 (1989).